J|A|C|S
ARTICLES
Published on Web 05/15/2002

Engineering the Structure and Magnetic Properties of Crystalline Solids via the Metal-Directed Self-Assembly of a Versatile Molecular Building Unit

Juan C. Noveron,* Myoung Soo Lah,† Rico E. Del Sesto, Atta M. Arif, Joel S. Miller, and Peter J. Stang*

Contribution from the Department of Chemistry, University of Utah, 315 S. 1400 E. RM 2020, Salt Lake City, Utah 84112-0850

Received January 4, 2002

Abstract: We report the supramolecular chemistry of several metal complexes of *N*-(4-pyridyl)benzamide (NPBA) with the general formula $[M_a(NPBA)_2A_bS_c]$, where M = Co^{2+}, Ni^{2+}, Zn^{2+}, Mn^{2+}, Cu^{2+}, Ag^{+}; A = NO_3^-, OAc^-; S = MeOH, H_2O; $a = 0, 1, 2$; $b = 0, 1, 2, 4$; and $c = 0, 2$. NPBA contains structural features that can engage in three modes of intermolecular interactions: (1) metal−ligand coordination, (2) hydrogen bonding, and (3) $\pi-\pi$ stacking. NPBA forms one-dimensional (1-D) chains governed by hydrogen bonding, but when reacted with metal ions, it generates a wide variety of supramolecular scaffolds that control the arrangement of periodic nanostructures and form 1- (**2**−**4**), 2- (**5**), or 3-D (**6**−**10**) solid-state networks of hydrogen bonding and $\pi-\pi$ stacking interactions in the crystal. Isostructural **7**−**9** exhibit a 2-D hydrogen bonding network that promotes topotaxial growth of single crystals of their isostructural family and generates crystal composites with two (**11**) and three (**12**) different components. Furthermore, **7**−**9** can also form crystalline solid solutions $(M,M')(NPBA)_2(NO_3)_2(MeOH)_2$ (M, M′ = Co^{2+}, Ni^{2+}, or Zn^{2+}, **13**−**16**), where mixtures of Co^{2+}, Ni^{2+}, and Zn^{2+} share the same crystal lattice in different proportions to allow the formation of materials with modulated magnetic moments. Finally, we report the effects that multidimensional noncovalent networks exert on the magnetic moments between 2 and 300 K of 1-D (**4**), 2-D (**5**), and 3-D (**7**, **8**, **10**, and **13**−**16**) paramagnetic networks.

Introduction

Designing the solid state with molecules that encode well-defined noncovalent motifs has recently become a rapidly growing area of research as it pursues to establish principles that will ultimately lead to the development of new state-of-the-art functional materials.[1−6] Among the noncovalent motifs, hydrogen bonding,[2,3] metal−ligand coordination,[5−7] and $\pi-\pi$ stacking[8−11] have been employed as synthetic paradigms to rationally design superstructures. In the design of crystalline solids, the formation of predetermined molecular networks of noncovalent interactions has been more successful than the prediction of the crystal structure.[12] Recent progress in this area has generated examples where the design of network structures produced crystals with (a) one-dimensional (1-D) molecular networks composed of hydrogen bonding,[13−15] metal−ligand coordination,[16−22] or a combination of these and other inter-

* Corresponding author. E-mail: stang@chem.utah.edu.
† Visiting scholar from the College of Science and Technology, 1271 Sa-1-dong, Ansan, Kyunggi-do, 425-791 Korea.

(1) Braga, D.; Grepioni, F.; Orpen A. G. *Crystal Engineering: From Molecules and Crystals to Materials*; NATO Science Series, Mathematical and Physical Sciences, Vol. 538; Kluwer Academic Publishers: Dordrecht, The Netherlands, 1999.
(2) Seddon, R. K.; Zaworotko, M. *Crystal Engineering: The Design and Application of Functional Solids*; NATO Science Series, Mathematical and Physical Sciences, Vol. 539; Kluwer Academic Publishers: Dordrecht, The Netherlands, 1999.
(3) Desiraju, G. *Crystal Engineering: The Design of Organic Solids*; Elsevier Science Publishers B.V.: Amsterdam, The Netherlands, 1989.
(4) Chin, D. N.; Zerkowski, J. A.; MacDonald, J. C.; Whitesides, G. M. *Organized Molecular Assemblies in the Solid State*; John Wiley and Sons: New York, 1999; pp 185−253.
(5) Fujita, M. *Molecular Self-Assembly—Organic versus Inorganic Approaches;* Structure and Bonding, Vol. 96; Springer-Verlag: Berlin Heidelberg, Germany, 2000.
(6) Lehn, J. M. *Supramolecular Chemistry—Concepts and Perspectives*; VCH: Weinheim, Germany, 1995.
(7) Leininger, S.; Olenyuk, B.; Stang, P. J. *Chem. Rev.* **2000**, *100*, 853.
(8) Hill, D. J.; Mio, M. J.; Prince, R. B.; Hughes, T. S.; Moore, J. S. *Chem. Rev*. **2001**, *101*, 3893.
(9) Lahiri, S.; Thompson, J. L.; Moore, J. S. *J. Am. Chem. Soc.* **2000**, *122*, 11315.
(10) Shetty, A. S.; Zhang, J.; Moore, J. S. *J. Am. Chem. Soc*. **1996**, *118*, 1019.
(11) Hunter, C. A.; Sanders, J. K. M. *J. Am. Chem. Soc*. **1990**, *112*, 5525.
(12) Desiraju, G. R. *Chem. Commun*. **1997**, 1475.
(13) Palacin, S.; Chin, D. N.; Simanek, E. E.; MacDonald, J. C.; Whitesides, G. M.; McBride, M. T.; Palmore, G. T. R. *J. Am. Chem. Soc.* **1997**, *119*, 11807.
(14) Schwiebert, K. E.; Chin, D. N.; MacDonald, J. C.; Whitesides, G. M. *J. Am. Chem. Soc*. **1996**, *118*, 4018.
(15) Chang, Y. L.; West, M. A.; Fowler, F. W.; Lauher, J. W. *J. Am. Chem. Soc.* **1993**, *115*, 5991.
(16) For a recent review see: Moulton, B.; Zaworotko, M. J. *Chem. Rev*. **2001**, *101*, 1629.
(17) Tabellion, F. M.; Seidel, S. R.; Arif, A. A.; Stang, P. J. *Angew. Chem., Int. Ed*. **2001**, *40*, 1529.
(18) Ellis, W. W.; Schmitz, M.; Arif, A. A.; Stang, P. J. *Inorg. Chem*. **2000**, *39*, 2547.
(19) Biradha, K.; Seward, C.; Zaworotko, M. J. *Angew. Chem., Int. Ed*. **1999**, *38*, 492.
(20) Kaes, C.; Hosseini, M. W.; Rickard, C. E. F.; Skelton, B. W.; White, A. H. *Angew. Chem., Int. Ed*. **1998**, *37*, 920.
(21) Goodgame, D. M.; Grachvogel, D. A.; Hitman, M. A.; Long, N. J.; Stratemeier, H.; White, A. J. P.; Wicks, J. L. M.; Williams, D. J. *Inorg. Chem*. **1998**, *37*, 6354.
(22) Carlucci, L.; Ciani, G.; Gudenberg, D. W. V.; Proserpio, D. M. *Inorg. Chem.* **1997**, *36*, 3812.

actions, referred to as hybrid interactions,[23−27] (b) 2-D networks composed either of hydrogen bonding,[28−35] metal−ligand coordination,[36−43] or hybrid interactions,[44−49] and (c) 3-D networks composed of hydrogen bonding[50−53] or metal−ligand coordination.[54−57] These approaches seek to establish connections between the molecular and supramolecular structures and look for molecular features such as functional groups that correspond with arrangements of molecules in crystals, a task that remains a considerable challenge at present.

We are exploring a strategy for the design of function in solid-state structures based on the design of molecules that use metal−ligand coordination, hydrogen bonding, and $\pi-\pi$ stacking interactions as directional motifs to guide the self-assembly of network structures. Herein we report the supramolecular chemistry along with its structure−property relationships of *N*-(4-pyridyl)benzamide (NPBA), Figure 1, as it utilizes several types of interactions to form crystals where the metal ions and solvent conditions used during the self-assembly process control the dimensional propagation of infinite hydrogen bonding and $\pi-\pi$ stacking interactions to produce solids with 1-, 2-, or 3-D noncovalent networks as illustrated in Scheme 1. We show that isostructural materials enable topotaxial as well as solid solution crystal growth with their isostructural members and result in crystalline heterostructures. We also demonstrate that topotaxial growth in these structures takes place preferentially along the direction of hydrogen bonding. Furthermore, formation of solid solutions with different metal ions enables the preparation of materials with modulated magnetic properties.

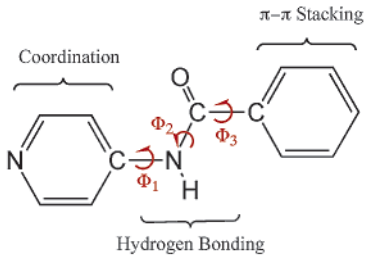

Figure 1. *N*-(4-Pyridyl)benzamide (NPBA).

Scheme 1. Graphic Representation of the Formation of 1-, 2-, and 3-D Networks of Noncovalent Interactions in Crystalline Solids

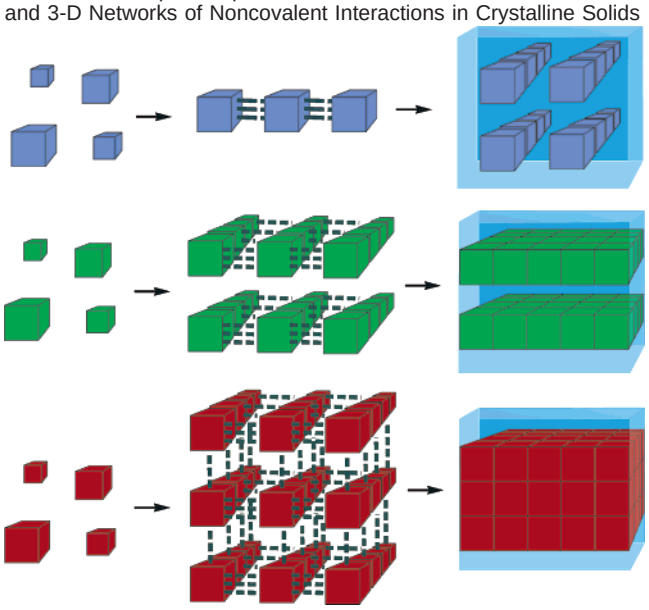

Experimental Section

General. Benzyl chloride, triethylamine, 4-aminopyridine, manganese(II) nitrate hexahydrate, cobalt(II) nitrate hexahydrate, nickel(II) nitrate hexahydrate, zinc(II) nitrate hydrate, manganese(II) acetate tetrahydrate, cobalt(II) acetate tetrahydrate, copper(II) acetate hydrate, zinc(II)acetate, and silver(I) acetate were used as received from commercial sources (Sigma-Aldrich or Lancaster). NMR spectra were obtained at room temperature with a Varian XL-300 spectrometer. Magnetic susceptibility measurements were made with a Quantum Design MPMS-5XL SQUID ac/dc magnetometer as previously described.[58] Elemental analysis was performed by Oneida Research Service, Whitesboro, NY, and Atlantic Microlab Inc., Norcross, GA. Single-crystal X-ray diffraction data for all the compounds were collected on a Nonius Kappa CCD diffractometer equipped with Mo Ka radiation ($\lambda = 0.71073$ Å).

Synthesis of NPBA. A solution of benzyl chloride (1.00 g, 7.12 mmol) and triethylamine (1.0 mL, 7.20 mmol) in 50 mL of chloroform

(23) Kuehl, C. K.; Tabellion, F. M.; Arif, A. M.; Stang, P. J. *Organometallics* **2001**, *20*, 1956.
(24) Gianneschi, N. C.; Tiekink E. R. T.; Rendina, L. M. *J. Am. Chem. Soc.* **2000**, *122*, 8474.
(25) Groeneman, R. H.; Macgillivray, L. R.; Atwood, J. L. *Inorg. Chem.* **1999**, *38*, 208.
(26) Braga, D.; Maini, L.; Grepioni, F. *Angew. Chem., Int. Ed.* **1998**, *37*, 2240.
(27) Burrows, A. D.; Chan, C. W.; Chowdhry, M. M.; McGrady, J. E.; Mingos, D. M. P. *Chem. Soc. Rev.* **1995**, 329.
(28) Kuduva, S. S.; Bläser, D.; Boese, R.; Desiraju, G. R. *J. Org. Chem.* **2001**, *66*, 1621.
(29) Muthuraman, M.; Masse, R.; Nicoud, J.; Desiraju, G. R. *Chem. Mater.* **2001**, *13*, 1473.
(30) Felix, O.; Hossein, M. W.; De Cian, A.; Fischer, J. *Chem. Commun.* **2000**, 281.
(31) Mascal, M.; Hansen, J.; Fallon, P. S.; Blake, A. J.; Heywood, B. R.; Moore, M. H.; Turkenburg, J. P. *Chem. Eur. J.* **1999**, *5*, 381.
(32) Aakeröy, C. B.; Nieuwenhuyzen M. *J. Am. Chem. Soc.* **1998**, *120*, 8986.
(33) Biradha, K.; Zaworotko, M. J. *J. Am. Chem. Soc.* **1998**, *120*, 6431.
(34) Aakeröy, C. B.; Hughes, D. P.; Nieuwenhuyzen M. *J. Am. Chem. Soc.* **1996**, *118*, 10134.
(35) Aoyama, Y.; Endo, K.; Anzai, T.; Yamaguchi, Y.; Sawaki, T.; Kobayahsi, K.; Kanehisa, N.; Hashimoto, H.; Kai, Y.; Masuda, H. *J. Am. Chem. Soc.* **1996**, *118*, 5562.
(36) Robson, R. *J. Chem. Soc., Dalton Trans.* **2000**, 3735.
(37) Kasai, K.; Aoyagi, M.; Fujita, M. *J. Am. Chem. Soc.* **2000**, *122*, 2140.
(38) Graham, P. M.; Pike, R. D.; Sabat, M.; Bailey, R. D.; Pennington, W. T. *Inorg. Chem.* **2000**, *39*, 5121.
(39) Biradha, K.; Hongo, Y.; Fujita, M. *Angew. Chem., Int. Ed.* **2000**, *39*, 3843.
(40) Biradha, K.; Mondal, A.; Moulton, B.; Zaworotko, M. J. *J. Chem. Soc., Dalton Trans.* **2000**, 3837.
(41) Batten, S. R.; Robson, R. *Angew. Chem., Int. Ed.* **1998**, *37*, 1460.
(42) Kumar, R. K.; Goldberg, I. *Angew. Chem., Int. Ed.* **1998**, *37*, 3027.
(43) Garner, G. B.; Venkataraman, D.; Moore, J. S.; Lee, S. *Nature* **1995**, *374*, 792.
(44) Groeneman, R. H.; MacGillivray, L. R.; Atwood, J. L. *Chem. Commun.* **1998**, 2735.
(45) Aakeröy, C. B.; Beatty, A. M.; Leinen, D. S. *Angew. Chem., Int. Ed.* **1999**, *38*, 1815.
(46) Choi, H. J.; Lee, T. S.; Suh, M. P. *Angew. Chem., Int. Ed.* **1999**, *38*, 1405.
(47) Aakeröy, C. B.; Beatty, A. M. *Chem. Commun.* **1998**, 1067.
(48) MacDonald, J. C.; Dorrestein, P. C.; Pilley, M. M.; Foote, M. M.; Lundburg, J. L.; Henning, R. W.; Schultz, A. J.; Manson, J. L. *J. Am. Chem. Soc.* **2000**, *122*, 11692.
(49) Aakeröy, C. B.; Beatty, A. M.; Leinen, D. S. *J. Am. Chem. Soc.* **1998**, *120*, 7383.
(50) Holman, K. T.; Pivotar, A. M.; Swift, J. A.; Ward, M. D. *Acc. Chem. Res.* **2001**, *34*, 107.
(51) Holman, K. T.; Martin, S. M.; Parker, D. P.; Ward, M. D. *J. Am. Chem. Soc.* **2001**, *123*, 4421.
(52) Kuduva, S. S.; Craig, D. C.; Nangia, A.; Desiraju, G. R. *J. Am. Chem. Soc.* **1999**, *121*, 1936.
(53) Thalladi, V. R.; Brasselet, S.; Weiss, H. C.; Blaser, D.; Katz, A. K.; Carrell, H. L.; Boese, R.; Zyss, J.; Nangia, A.; Desiraju, G. R. *J. Am. Chem. Soc.* **1998**, *120*, 2563.
(54) Prior, T. J.; Rosseinsky, M. J. *Chem. Commun.* **2001**, 495.
(55) Noro, S.; Kitagawa, S.; Kondo, M.; Seki, K. *Angew. Chem., Int. Ed.* **2000**, *39*, 2082.
(56) Posner, Y. D.; Dahal, S.; Goldberg, I. *Angew. Chem., Int. Ed.* **2000**, *39*, 1288.
(57) Kondo, M.; Okubo, T.; Asami, A.; Noro, S.; Yoshitomi, T.; Kitagawa, S.; Ishii, T.; Matsuzaka, H.; Seki, K. *Angew. Chem., Int. Ed.* **1999**, *38*, 140.
(58) Brandon, E. J.; Rittenberg, D. K.; Arif, A. M.; Miller, J. S. *Inorg. Chem.* **1998**, *37*, 3376.

was prepared and chilled to 4 °C in an ice bath for 5 min. Then, 4-aminopyridine (0.669 g, 7.12 mmol) was added slowly to the cold solution over a period of 10 min. The reaction was allowed to stir at room temperature overnight and upon concentration a white precipitate was obtained and identified as the product. The solid was filtered and washed several times with cold chloroform. Yield 1.03 g (79%). ^{1}H NMR spectrum (d_6-DMSO, 300 MHz) δ from TMS: 7.63 (m, 3H, Bz), 7.78 (d, 2H, Py), 7.95 (d, 2H, *o*-Bz), 8.47 (d, 2H, Py), 10.60 (s, NH). ^{13}C NMR spectrum (d_6-DMSO, 62.5 MHz): 114.70, 128.56, 129.15, 132.76, 134.96, 146.66, 150.97, 167.19.

Preparation of [Ag(NPBA)$_2$](NO$_3$) (2). A solution of NPBA (20 mg, 0.10 mmol) in 5 mL of methanol was added to a 5 mL methanolic solution of silver nitrate (8.45 mg, 0.05 mmol) and the mixture was stirred for 30 min in the dark. Diffusion of diethyl ether into the reaction mixture for 48 h generated large colorless crystals of **2**. Yield 87%. Anal. Calcd for $C_{24}H_{20}N_5O_5Ag$: C 50.90, H 3.56, N 12.37. Found: C 50.39, H 3.87, N 12.94.

Preparation of Zn(NPBA)$_2$(OAc)$_2$ (3) and Zn$_2$(NPBA)$_2$(OAc)$_2$ (6). A solution of NPBA (20 mg, 0.10 mmol) in 5 mL of methanol was added to a 5 mL methanolic solution of zinc(II) acetate (12.4 mg, 0.05 mmol) and allowed to stir for 12 h. Next, the solution was allowed to evaporate slowly over a period of 48 h during which it generated 15.9 mg (55.3%; colorless needle shaped crystals) of **3** and 7.3 mg (38.6%; colorless prismatic crystals) of **6** that were separated by hand according to their crystal shape. Anal. Calcd for $C_{28}H_{26}N_4O_6Zn$ (**3**): C 57.99, H 4.52, N 9.66. Found: C 57.39, H 4.55, N 9.66. Anal. Calcd for $C_{32}H_{32}N_4O_{10}Zn_2$ (**6**): C 50.35, H 4.23, N 7.34. Found: C 50.39, H 4.37, N 7.54.

Preparation of Cu(NPBA)$_2$(OAc)$_2$ (4). A solution of NPBA (20 mg, 0.10 mmol) in 5 mL of methanol was added to a 5 mL methanolic solution of copper(II) acetate (12.5 mg, 0.05 mmol) and allowed to stir for 12 h. Slow evaporation of this methanol solution generated 20.3 mg (69.2%; purple plate crystals) of **4**. Anal. Calcd for $C_{28}H_{26}N_4O_6Cu$: C 58.18, H 4.53, N 9.69. Found: C 58.39, H 4.57, N 9.74.

Preparation of Co(NPBA)$_2$(OAc)$_2$(H$_2$O)$_2$ (5). A solution of NPBA (20 mg, 0.10 mmol) in 5 mL of ethanol was added to a 5 mL ethanolic solution of cobalt(II) acetate hexahydrate (12.5 mg, 0.05 mmol) and allowed to stir for 12 h. Slow evaporation of the solution during 48 h gave 26.7 mg (86.7%; pale reddish needles) of **5**. Anal. Calcd for $C_{28}H_{30}N_4O_8Co$: C 55.18, H 4.96, N 9.19. Found: C 55.39, H 4.87, N 9.18.

Preparation of M(NPBA)$_2$(NO$_3$)$_2$(MeOH)$_2$ (M = Co^{2+} (7), Ni^{2+} (8), Zn^{2+} (9)). A solution of NPBA (20 mg, 0.10 mmol) in 5 mL of methanol was added to a 5 mL methanolic solution of the corresponding metal nitrate (0.05 mmol). The mixture was heated at 60 °C for 5 min and then allowed to stand at room temperature for 24 h. During this time, microcystals corresponding to compounds **7**−**9** were formed. Yield: **7**, 95%; **8**, 92%; **9**, 87%. Diffusion of diethyl ether into a dilute methanolic solution of the complexes containing seed crystals of any one of **7**−**9** generated large crystals. Anal. Calcd for $C_{26}H_{28}N_6O_{10}Co$ (**7**): C 48.5, H 4.85, N 13.75. Found: C 48.32, H 4.65, N 13.90. Anal. Calcd for $C_{26}H_{28}N_6O_{10}Ni$ (**8**): C 48.60, H 4.85, N 13.75. Found: C 48.50, H 4.82, N 13.70. Anal. Calcd for $C_{26}H_{28}N_6O_{10}Zn$ (**9**): C 48.60, H 4.85, N 13.75. Found: C 48.45, H 4.80, N 13.8.

Preparation of Mn(NPBA)$_2$(NO$_3$)$_2$(H$_2$O)$_2$ (10). A solution of NPBA (20 mg, 0.10 mmol) in 5 mL of ethanol was added to a 5 mL ethanol: water (80:20) solution of manganese(II) nitrate hydrate (14.3 mg, 0.05 mmol) and allowed to stir for 1 h. Slow evaporation of the solution during 48 h gave 30.58 mg (97%; pale yellow needles) of **10**. Anal. Calcd for $C_{24}H_{24}N_6O_{10}Mn$: C 47.10, H 3.93, N 13.73. Found: C 47.00, H 3.97, N 13.83.

Formation of Crystal Composites 11 and 12. The crystal composite **11** was prepared by seeding a 1.5 mM methanol−toluene (60:40, v/v) solution of Ni-complex **8** with single crystals of Co-complex **7** followed by diffusion of diethyl ether for 36 h. The triple crystal composite **12** was prepared by seeding a 1.5 mM methanol−toluene (60:40, v/v) solution of Co-complex **7** with single crystals of Zn-complex **9** followed by diffusion of diethyl ether for 12 h. Next, the resulting two composite crystals were used as seeds in a freshly prepared 1.5 mM methanol−toluene (60:40, v/v) solution of the Ni-complex **8** followed by diffusion of diethyl ether for another 12 h.

Formation of Solid Solutions 13−16. The solid solutions of paramagnetic mixed crystals **13**−**16** were prepared by mixing warm 1.5 mM methanolic solutions of mixtures of Co-complex **7** and Ni-complex **8** in a ratio of 75:25 for **13**, 50:50 for **14**, 25:75 for **15**, and 50:50 of Ni-complex **8** and Zn-complex **9** for **16** followed by diethyl ether diffusion into the respective solutions for 48 h.

Crystal Structure Determination. The data collection was carried out at 200(1) K and the range for data collection was 3.44 to 27.89° in θ. The data were corrected for absorption using the DENZO-SMN program.[59] The structures were solved by a combination of direct methods and heavy atom method using SIR 97.[60] For the final structural refinement SHELXL97 was used.[61] All of the non-hydrogen atoms were refined with an anisotropic displacement coefficient. Hydrogen atoms were located and refined isotropically using SHELXL97. Pertinent crystallographic data are listed in Table 1.

Results and Discussion

Design Principles. To explore the supramolecular trends exhibited by molecules that can engage simultaneously in metal−ligand coordination, hydrogen bonding, and $\pi-\pi$ stacking interactions, *N*-(4-pyridyl)benzamide (NPBA) was prepared and its coordination chemistry and crystalline packing behavior under varying conditions was investigated. NPBA consists of three structural parts: (1) a pyridyl group that can coordinate to a metal, (2) a carboxamide group, which can have hydrogen bonding interactions through the amide nitrogen atom as well as via the carbonyl oxygen atom, and (3) a phenyl group, which can be involved in $\pi-\pi$ stacking interactions (Figure 1). We hypothesized that because NPBA, as a consequence of conjugation, has planar functional groups, its reactions with various metal ions capable of forming complexes with different coordination numbers and geometries would generate molecular scaffolds with unique directional hydrogen bonding and $\pi-\pi$ stacking motifs that might direct via self-assembly well-defined structural motifs.

In our design, the metal centers (1) assemble the ligands into the required geometrical orientations to promote unique intermolecular connections and (2) pre-organize solvent and counterion via coordination to assist in the formation of infinite ensembles of hydrogen bonding interactions.

Supramolecular Patterns of Crystalline Networks 1−10. A systematic investigation of the supramolecular structural trends of NPBA under various reactions conditions revealed that depending on the coordination number, geometry of the metal ions, and the solvent, a variety of crystalline motifs (**2**−**10**) can be generated that comprise 1-, 2-, or 3-D solid-state networks of hydrogen bonding and $\pi-\pi$ stacking interactions. The hydrogen bonding networks are primarily formed via the directional interactions of the carboxamide group of NPBA and counterions or solvent molecules coordinated to the metal ions. The hydrogen bonding parameters are listed in Table 2. The

(59) Otwinowski, Z.; Minor, W. *Methods Enzymol.* **1997**, *276*, 307.
(60) *SIR97* (Relase 1.02); A program for automatic solution and refinement of crystal structure; Altomare, A.; Burla, M. C.; Camalli, M.; Cascarano, G.; Giacovazzo, C.; Guagliardi, A.; Moliteni, A. G. G., Polidori, G.; Spagna, R.
(61) *SHELX97* [Includes SHELX97, SHELXL97, CIFTAB]; Programs for Crystal Structure Analysis (Release 97-2); Sheldrick, G. M.; University of Göttingen: Göttingen, Germany, 1997.

Table 1. Crystal Data and Structure Refinement

identification code	NPBA 1	Ag-complex **2**	Zn-complex **3**	Cu-complex **4**	Co-complex **5**	Zn-complex **6**
empirical formula	$C_{12}H_{10}N_2O$	$C_{24}H_{20}N_5O_5Ag$	$C_{28}H_{26}N_4O_6$ Zn	$C_{28}H_{26}$ N_4O_6Cu	$C_{28}H_{30}N_4O_8Co$	$C_{32}H_{32}N_4O_{10}Zn_2$
formula weight	198.22	566.32	579.90	578.07	609.49	763.36
space group	$P2_1/c$	$P\bar{1}$	$C2/c$	$P\bar{1}$	$P2_1/c$	$C2/c$
unit cell dimens.						
a (Å)	5.6830(2)	7.4427(2)	17.6920(3)	8.0203(2)	15.8579(4)	19.8901(3)
b (Å)	11.1380(3)	8.8081(2)	10.2177(2)	8.7561(3)	5.4924(1)	12.3626(3)
c (Å)	15.2124(6)	17.2876(5)	15.1922(3)	9.8058(3)	16.0201(5)	15.0476(3)
α (deg)	90	93.6327(9)	90	76.776(2)	90	90
β (deg)	95.0784(13)	90.9294(10)	115.4011(12)	75.4011(18)	110.4856(11)	113.9569(15)
γ (deg)	90	94.3935(8)	90	83.5565(14)	90	90
V (Å^3)	959.12(6)	1127.45(5)	2480.82(8)	647.63(3)	1307.08(6)	3381.34(12)
independent reflcns	2187	5034	2928	3022	2961	3847
goodness-of-fit on F^2	1.028	1.046	1.025	1.046	1.030	1.003
final R indices [$I > 2\sigma(I)$]						
$R1$,[a] $wR2$[b]	0.0380, 0.0878	0.0323, 0.0659	0.0388, 0.0921	0.0459, 0.0861	0.0321, 0.0753	0.0389, 0.0816

identification code	Co-complex **7**	Ni-complex **8**	Zn-complex **9**	Mn-complex **10**	Co:Ni-composite **11**
empirical formula	$C_{26}H_{28}N_6O_{10}Co$	$C_{26}H_{28}N_6O_{10}Ni$	$C_{26}H_{28}N_6O_{10}Zn$	$C_{24}H_{24}N_6O_{10}Mn$	$C_{26}H_{28}N_6O_{10}Co_{0.5}Ni_{0.5}$
formula weight	643.47	643.25	649.91	611.43	643.47
space group	$P2_1/c$	$P2_1/c$	$P2_1/c$	$P\bar{1}$	$P2_1/c$
unit cell dimens.					
a (Å)	7.4471(2)	7.4380(2)	7.4389(3)	7.4848(2)	7.4425(3)
b (Å)	12.6393(2)	12.6144(5)	12.6873(2)	9.1264(3)	12.6362(5)
c (Å)	14.7616(4)	14.7117(5)	14.7479(5)	10.0961(3)	14.7425(8)
α (deg)	90	90	90	75.4420(16)	90
β (deg)	97.8869(14)	97.618(2)	97.9708(12)	73.0274(14)	97.8068(17)
γ (deg)	90	90	90	82.5842(12)	90°
V (Å^3)	1376.31(6)	1368.15(8)	1378.45(8)	637.28(3)	1373.61(11) Å^3
independent reflcns	3153	3122	3110	2842	3162
goodness-of-fit on F^2	1.042	1.031	1.039	1.009	1.042
final R indices [$I > 2\sigma(I)$]					
$R1$,[a] $wR2$[b]	0.0337, 0.0748	0.0362, 0.0778	0.0334, 0.0764	0.0481, 0.0789	0.0337, 0.0748

[a] $R1 = \sum(||F_o| - |F_c||)/\sum|F_o|$. [b] $wR2 = [\sum(w(F_o^2 - F_c^2)^2)/\sum(F_o^2)^2]^{1/2}$, and S = goodness-of-fit on $F^2 = [\sum(w(F_o^2 - F_c^2)^2/(n - p)]^{1/2}$, where n is the number of reflections and p is the number of parameters refined.

Table 2. Hydrogen Bonds (Å and deg) in **1**−**10**[a]

	D–H···A	d(D···A)	∠(DHA)	
NPBA **1**	N−H(Amido)···N(Pyridyl)	3.041(2)	142(1)	a
Ag-complex **2**	N−H(Amido)···O(Nitrate)	2.936(2)	169(3)	a
	N−H(Amido)···O(Nitrate)	3.114(3)	157(2)	a
Zn-complex **3**	N−H(Amido)···O(Acetate)	2.916(2)	161(2)	a
Cu-complex **4**	N−H(Amido)···O(Acetate)	2.904(3)	161(2)	a
Co-complex **5**	O−H(H_2O)···O(Acetate)	2.760(2)	160(2)	b
	N−H(Amido)···O(Amide)	3.334(2)	158(2)	a
	O−H(H_2O)···O(Acetate)	2.605(2)	171(2)	a
Zn-complex **6**	N−H(Amido)···O(Acetate)	2.908(3)	162(3)	a
Co-complex **7**	O−H(MeOH)···O(Nitrate)	2.822(2)	135(2)	b
	N−H(Amido)···O(Nitrate)	3.034(2)	155(2)	a
	O−H(MeOH)···O(Amide)	2.834(2)	144(2)	a
Ni-complex **8**	O−H(MeOH)···O(Nitrate)	2.802(2)	137(2)	b
	N−H(Amido)···O(Nitrate)	3.053(2)	153(2)	a
	O−H(MeOH)···O(Amide)	2.849(2)	142(3)	a
Zn-complex **9**	O−H(MeOH)···O(Nitrate)	2.861(2)	130(2)	b
	N−H(Amido)···O(Nitrate)	3.048(2)	154(2)	a
	O−H(MeOH)···O(Amide)	2.821(2)	148(2)	a
Mn-complex **10**	O−H(H_2O)···O(Nitrate)	2.847(2)	121(2)	b
	N−H(Amido)···O(Nitrate)	3.012(2)	163(2)	a
	O−H(H_2O)···O(Amide)	2.730(2)	172(2)	a
	O−H(H_2O)···.O(Nitrate)	2.888(2)	160(2)	a

[a] A, acceptor; D, donor; a, intermolecular; b, intramolecular.

Table 3. $\pi-\pi$ Stacking Interactions and Distances (Å) in **2**−**10**[a]

	Type I		Type II	Type III	Type IV	Type V
	Am−Py, Am		Py	Ph−Am	Ph−Py	Ph−Am−Py
	Py	Py	Py	Am−Ph	Py−Ph	Py−Am−Ph
Ag-complex **2**	3.43	3.61				
Zn-complex **3**			3.50			
Cu-complex **4**			3.44			
Co-complex **5**				3.64, 3.63		
Zn-complex **6**					3.42, 3.42	
Co-complex **7**				3.41, 3.45		3.56, 3.60
Ni-complex **8**				3.41, 3.45		3.56, 3.62
Zn-complex **9**				3.42,3.46		3.56, 3.62
Mn-complex **10**					3.63, 3.55	

[a] Am, carboxamide group; Ph, phenyl group; Py, pyridyl group.

$\pi-\pi$ stacking interactions are formed between various parts of the resonant structure of NPBA of the molecular units and are categorized according to the extent of $\pi-\pi$ overlap that occurs between the aromatic groups as Types I−V, where Type I represents only minor $\pi-\pi$ stacking and Types II−V correspond to increasingly larger degrees of $\pi-\pi$ stacking. The bonding parameters for the five types of $\pi-\pi$ stacking interactions are shown collectively in Table 3.

One-Dimensional Solid-State Networks. To propagate noncovalent interactions only along one direction, each unit must have two-point interactions with two adjacent neighbors. NPBA **1** epitomizes this model. It exhibits a two-point contact per unit that can result in 1-D hydrogen bonding networks where the carboxamide NH moieties and the pyridyl groups from adjacent molecular units propagate NH···N contacts of 3.04 Å along *b*

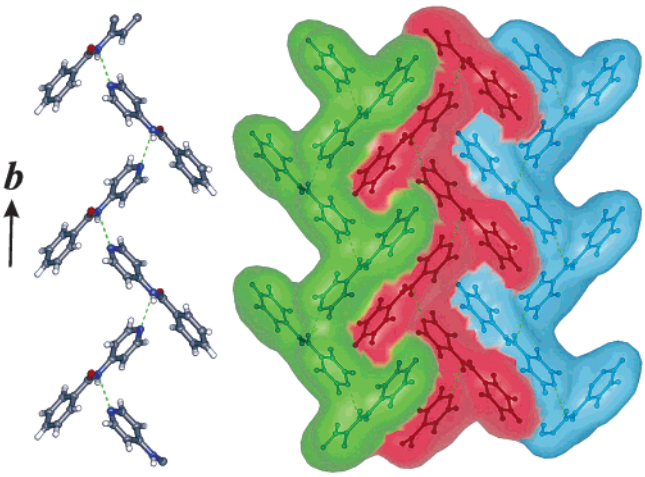

Figure 2. Structure of **1**. NPBA molecules form 1-D hydrogen bonding networks along *b*.

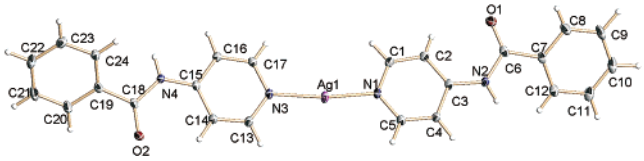

Figure 3. Structure of $[Ag(NPBA)_2](NO_3)$, **2**.

(Figure 2 and Table 2). Despite the presence of phenyl moieties in NPBA, **1** does not exhibit $\pi-\pi$ stacking interactions. We examined the interactions of NPBA with metals known to form complexes with low coordination numbers (<6) such as Ag(I), Zn(II), and Cu(II) centers and obtained **2**−**4**, derived from the hydrates of $Ag(NO_3)$, $Zn(OAc)_2$, and $Cu(OAc)_2$, respectively. These structures comprise infinite 1-D tape-like networks formed by concomitant hydrogen bonding and $\pi-\pi$ stacking interactions. Although these structures exhibit more than two-point contacts per unit, these interactions occur between two adjacent neighbors, and hence, form 1-D networked solids.

trans-$[Ag(NPBA)_2](NO_3)$ (**2**), Figure 3, lacks solvent, and has a 1-D noncovalent network composed of two hydrogen bonding contacts and two types of $\pi-\pi$ stacking interaction between the molecular units. The hydrogen bond interactions manifested by N−H···O contacts of 2.94 and 3.11 Å involve the four amide N(4)H groups in two adjacent NPBA's and the oxygen atoms of two bridging nitrate ions (Figure 4a and Table 2). The hydrogen bonding interactions result in the formation of a dimer that acts as a new unit that engages in two forms of Type I $\pi-\pi$ stacking interactions, one *within* the dimers (amide−Py···Py 3.43 Å, Figure 4b) and the other *between* the dimers (amide···Py 3.61 Å, Figure 4c), Table 3. Together, these associations generate infinite 1-D networks of noncovalent interactions that propagate along *a*.

When NPBA is reacted with zinc(II) acetate in methanol, **3** and **6** form simultaneously in 55% and 39% yields, respectively. $Zn(NPBA)_2(OAc)_2$ (**3**) is tetrahedral with two monodentate acetates (Figure 5), and has a 1-D network arising from hydrogen bonds and $\pi-\pi$ stacking interactions along *c*. The $Zn_2(NPBA)_2(OAc)_2$ (**6**) exhibits a 3-D noncovalent network system that will be discussed in a later section. The noncoordinating oxygen atoms O(3) of the acetate ions hydrogen bond

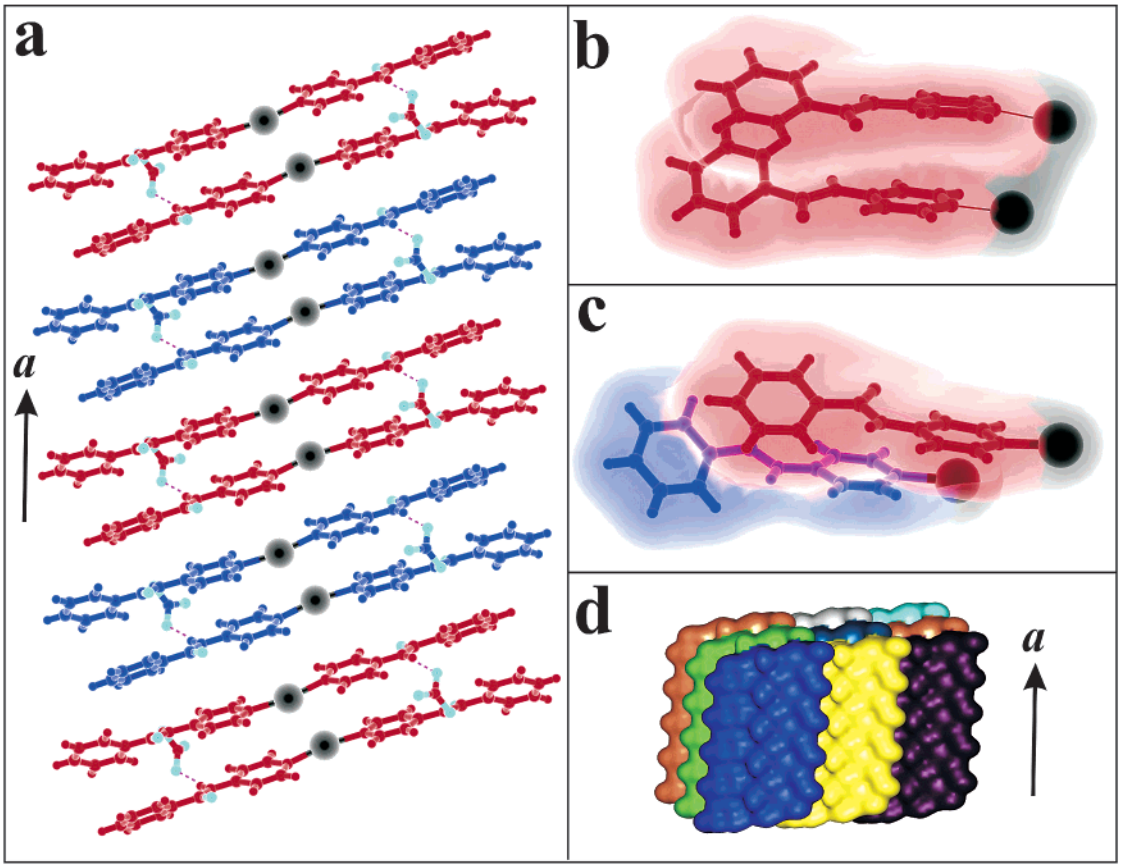

Figure 4. $[Ag(NPBA)_2](NO_3)$, **2**. (a) Dimeric units of **2** (red and blue sets) propagate $\pi-\pi$ stacking interactions along *a*. (b and c) Type I $\pi-\pi$ stacking interactions. (d) van der Waals surface of $\pi-\pi$ stacked rows in **2** (unique colors) as viewed from *b*.

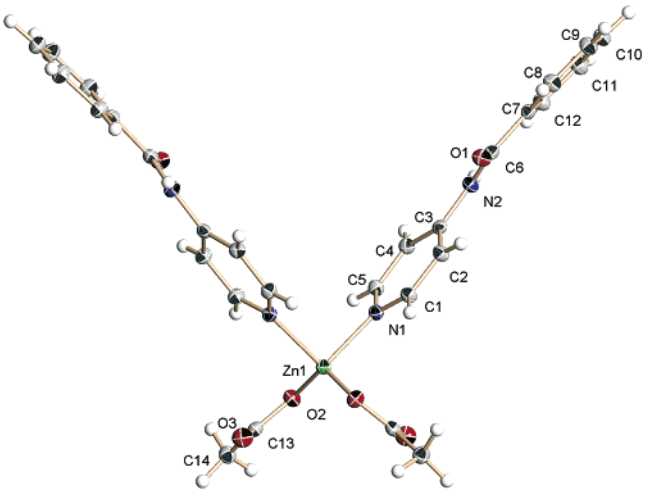

Figure 5. Structure of $Zn(NPBA)_2(OAc)_2$, **3**.

with the amide N(2)H groups from two adjacent zinc complexes that are opposite to one another and have N−H···O contacts of 2.91 Å (Figure 6a and Table 2), which propagates along *c*. Additionally, there are two $\pi-\pi$ stacking interactions between the pyridyl groups that are already involved in hydrogen bonding. The $\pi-\pi$ stacking interactions of the Py···Py moieties (Type II) have average inter-ring contacts of 3.50 Å and also propagate along *c* through the same networks formed by the hydrogen bonds (Figure 6b,c and Table 3).

Square-planar *trans*-$Cu(NPBA)_2(OAc)_2$ (**4**, Figure 7) has a parallel hydrogen bonding and $\pi-\pi$ stacking system that generates a tape-like 1-D network along *a*. The hydrogen bonding interactions occur between the amide protons N(2)H and the noncoordinating oxygen atoms O(3) of the acetates from the next adjacent units and have N−H···O contacts of 2.90 Å (Figure 8a and Table 2). The $\pi-\pi$ stacking interactions are similar to **3** and consist of Type II $\pi-\pi$ interactions between the pyridyl moieties of adjacent units with average inter-ring contacts of 3.44 Å (Figure 8b and Table 3).

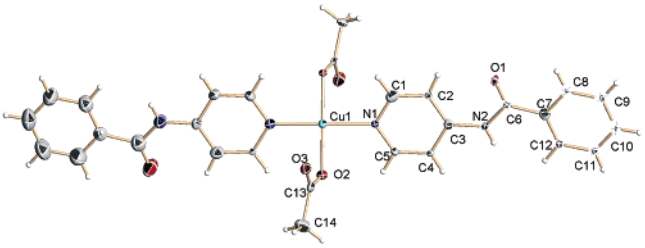

Figure 7. Structure of $Cu(NPBA)_2(OAc)_2$, **4**.

Two-Dimensional Solid-State Networks. To propagate noncovalent interactions in a plane to generate lamellar (2-D) networks, each unit must make at least three point interactions with at least three adjacent neighbors. We examined the interactions of NPBA with metals known to form six-coordinate complexes such as Mn(II), Co(II), and Ni(II) centers in order to promote the coordination of solvent molecules that could assist in the formation of more intricate noncovalent networks. We obtained a 2-D network structure, **5**, derived from the hydrate of $Co(OAc)_2$. This structure exhibits ten-point noncovalent contacts between each unit and four adjacent neighbors and such interactions propagate in 2-D to form lamellar networks. Reactions of NPBA with the corresponding nitrate salts of the aforementioned metal ions generated structures with 3-D noncovalent networks (**7**−**10**) and will be discussed in the next section.

Octahedral *trans*-$Co(NPBA)_2(OAc)_2(H_2O)_2$ (**5**, Figure 9) exhibit packing in which 1-D hydrogen bonded networks propagate perpendicular to the 1-D $\pi-\pi$ stacking networks and collectively form 2-D noncovalent networks. The hydrogen bonding networks are comprised of intramolecular and intermolecular hydrogen bonding interactions. Intramolecular hydrogen bond interactions occur between the O(2)H1 atoms of the coordinated water molecules and the noncoordinating oxygen atoms of the acetate groups O(3). Intermolecular hydrogen bond interactions occur between the same coordinated water O(2)-H2 and the oxygen atoms O(4) of the acetates coordinated to

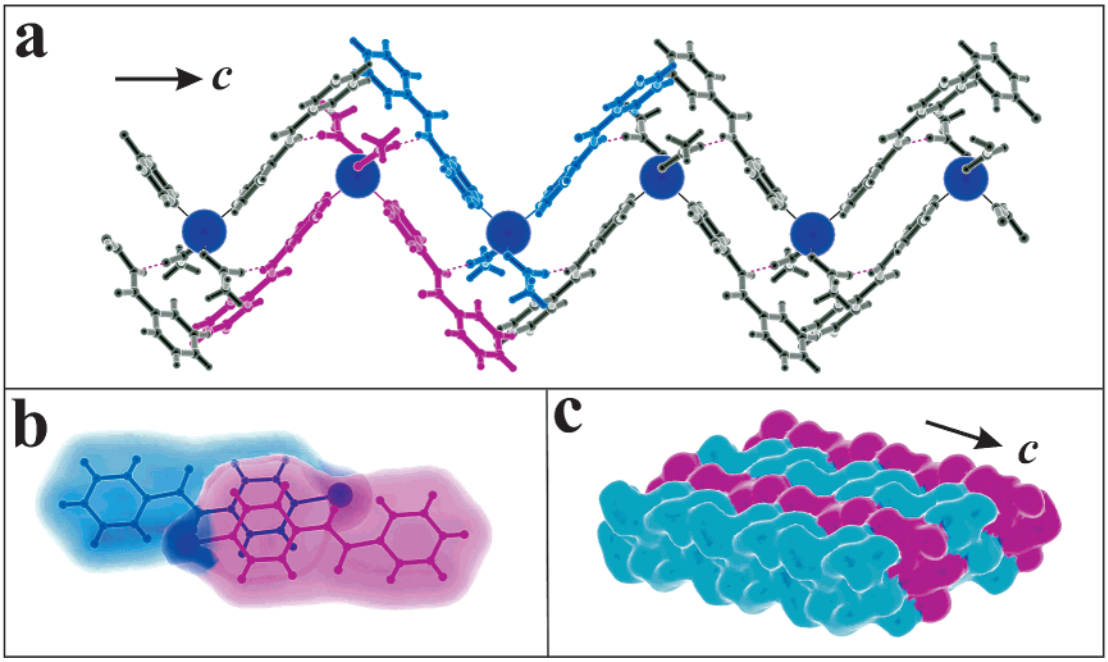

Figure 6. $Zn(NPBA)_2(OAc)_2$,**3**. (a) Units of **3** form dimeric rows (red and blue) that propagate hydrogen bonding and $\pi-\pi$ stacking interactions along *c*. (b) Type II $\pi-\pi$ stacking interactions. (c) van der Waals surface of 1-D noncovalent networks in **3**.

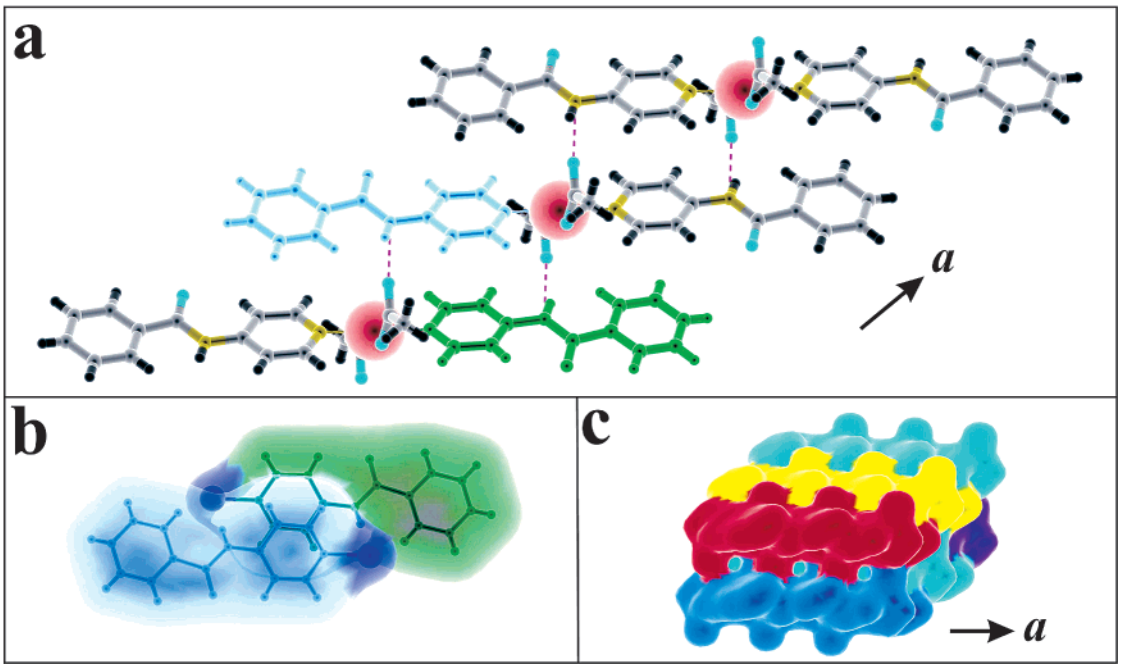

Figure 8. Cu(NPBA)$_2$(OAc)$_2$, **4**. (a) Units of **4** propagate hydrogen bonding and $\pi-\pi$ stacking interactions along *a*. (b) Type II $\pi-\pi$ stacking interactions. (c) van der Waals surface of 1-D noncovalent networks (unique colors) in **4**.

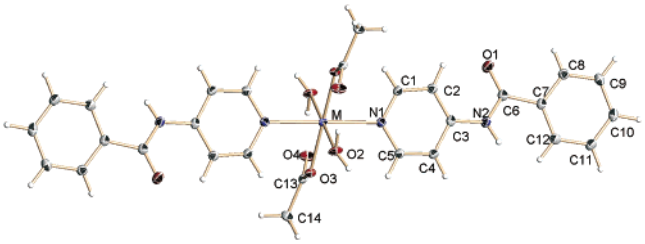

Figure 9. Structure of Co(NPBA)$_2$(OAc)$_2$(H$_2$O)$_2$, **5**.

the two adjacent metal complexes that are positioned opposite to one another with average O−H···O contacts of 2.60 Å. The other intermolecular hydrogen bond interactions are between the amide groups N(2)H and the carbonyl groups C═O(1), also from the same adjacent units, and have N−H···O average contacts of 3.33 Å. All the hydrogen bond interactions propagate along *b* and form tape-like 1-D networks (Figure 10a and Table 2). Perpendicular to the hydrogen bonding networks are 1-D $\pi-\pi$ stacking interactions. They consist of the stacking of the benzamido moieties of NPBA (Ph−Am···Ph−Am, Type III)

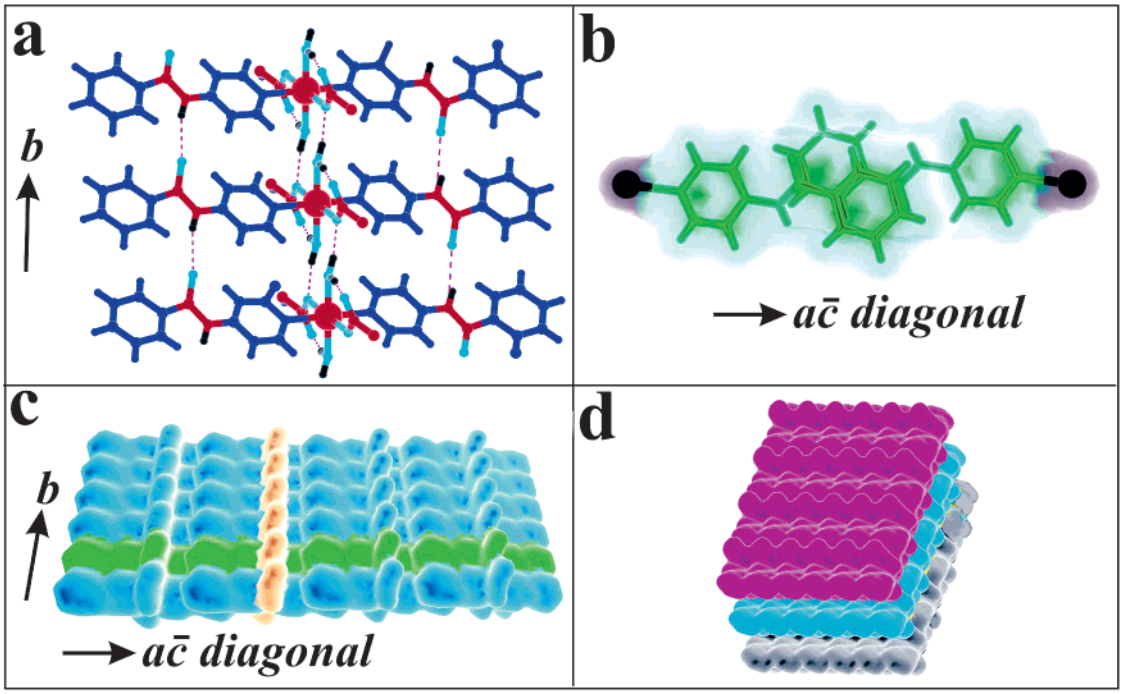

Figure 10. Co(NPBA)$_2$(OAc)$_2$(H$_2$O)$_2$, **5**. (a) 1-D hydrogen bonding network along *b*. (b) Type III $\pi-\pi$ stacking. (c) 1-D Type III $\pi-\pi$ stacking networks (green) propagate perpendicular to hydrogen bonding networks (yellow). (d) van der Waals surfaces of 2-D sheet networks (unique colors) of concomitant noncovalent interactions.

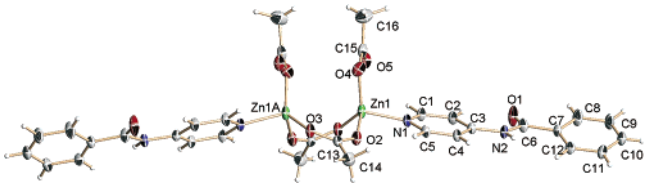

Figure 11. Structure of $Zn_2(NPBA)_2(OAc)_2$, **6**.

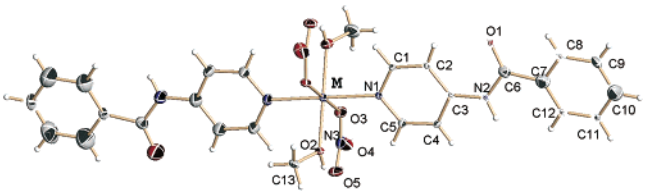

Figure 13. Structure of $M(NPBA)_2(NO_3)_2(MeOH)_2$, M = Co^{2+} (**7**), Ni^{2+} (**8**), and Zn^{2+} (**9**).

with average inter-ring contacts of 3.63 Å and propagate along the $a\bar{c}$ diagonal (Figure 10b,c and Table 3). The $\pi-\pi$ stacking forms 1-D rows that do not interact with one another, but together with the hydrogen bonding system generates 2-D sheet-networks parallel to the $a\bar{c}$ diagonal plane, Figure 10.

Three-Dimensional Solid-State Networks. 3-D interconnected networks require that each unit make at least four-point interactions with at least four adjacent molecular neighbors. The $Zn_2(NPBA)_2(OAc)_2$ (**6**) epitomizes the simplest case. It exhibits a 3-D network that is formed from 1-D hydrogen bonding and $\pi-\pi$ stacking networks that are perpendicular to one another and comprise a basic unit that interacts with only four adjacent neighbors via two $\pi-\pi$ stacking and four hydrogen bonding interactions. Complex **6** consist of a dinuclear Zn(II) complex where each tetrahedral metal center has one NPBA, one monodentate acetate, and two bridging acetates (Figure 11). Intermolecular hydrogen bonds are manifested as N−H···O contacts of 2.91 Å between the amide groups N(2)H and one of the noncoordinating oxygen atoms O(5) of the monodentate acetates from the adjacent complexes and propagate in one-dimension along *c* (Figure 12b and Table 2). The Type IV $\pi-\pi$ stacking interactions consist of the stacking of the phenyl and pyridyl moieties (Py···Py 3.42 Å) from adjacent complexes that propagate these interactions along the $a\bar{c}$ diagonal (Figure 12a and Table 3). These two 1-D networks interact with one another in a zigzag fashion along *b* (Figure 12d), and together generate a 3-D noncovalent interconnected solid.

Reactions of NPBA with the corresponding nitrate salts of Co(II), Ni(II), Zn(II), and Mn(II) form **7**−**10**, respectively, which exhibit more intricate 3-D networks of hydrogen bonding and $\pi-\pi$ stacking interactions. *trans*-$M(NPBA)_2(NO_3)_2(MeOH)_2$ **7**−**9** (Figure 13) are isostructural and interact with eight adjacent neighbors via twelve noncovalent connections to generate 2-D networks of hydrogen bonding that run perpendicular to another 2-D $\pi-\pi$ stacking array. The hydrogen bonding system in these structures is composed of intramolecular and intermolecular interactions. Intramolecular hydrogen bonding occurs between the coordinated methanol O(2)H and the noncoordinated oxygen atoms O(5) of the nitrates from the same metal complex with average O−H···O contacts of 2.82 Å. The intermolecular hydrogen bonds consist of interactions between the oxygen

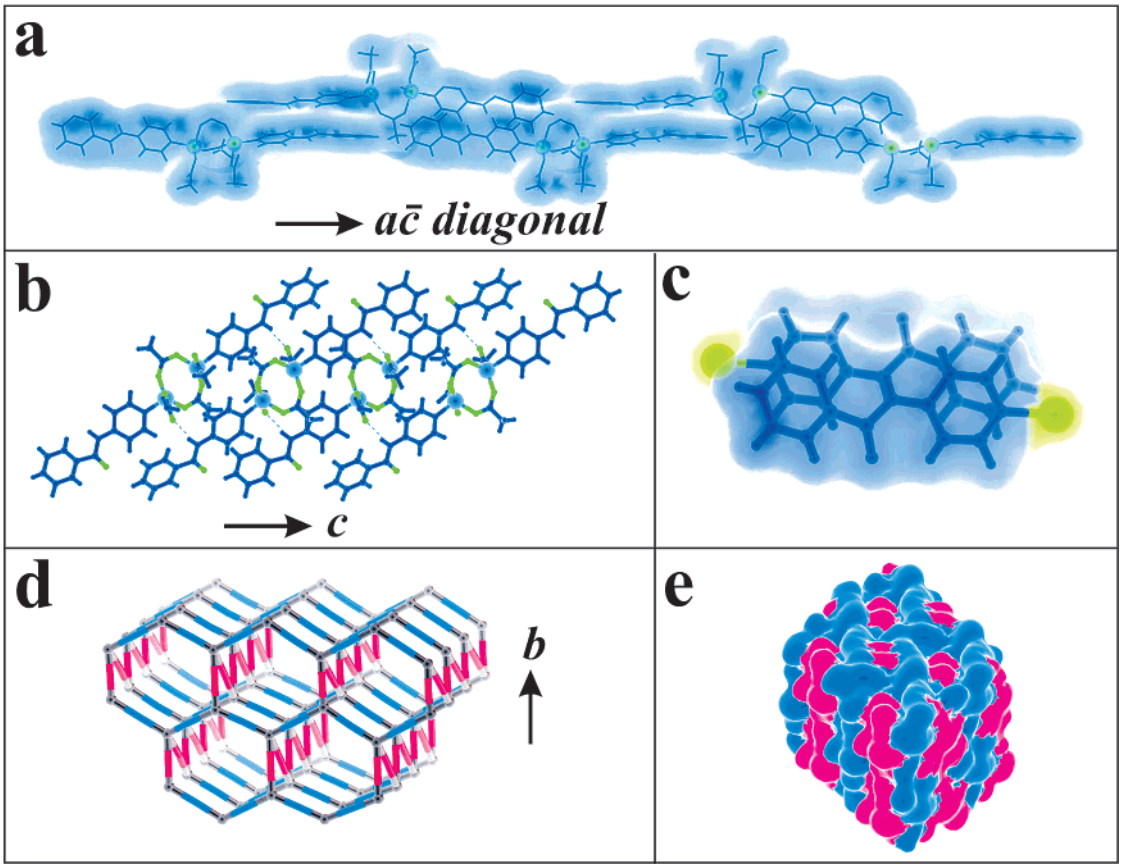

Figure 12. $Zn_2(NPBA)_2(OAc)_2$, **6**. (a) 1-D Type IV $\pi-\pi$ stacking networks propagate in a zigzag fashion along the $a\bar{c}$ diagonal. (b) The 1-D hydrogen bonding network propagates in a zigzag fashion along *c*. (c) Type IV $\pi-\pi$ stacking. (d) Schematic structure of **7** (red are hydrogen bonding networks and blue are $\pi-\pi$ stacking networks). (e) van der Waals surfaces of the 3-D noncovalent networks in **7**.

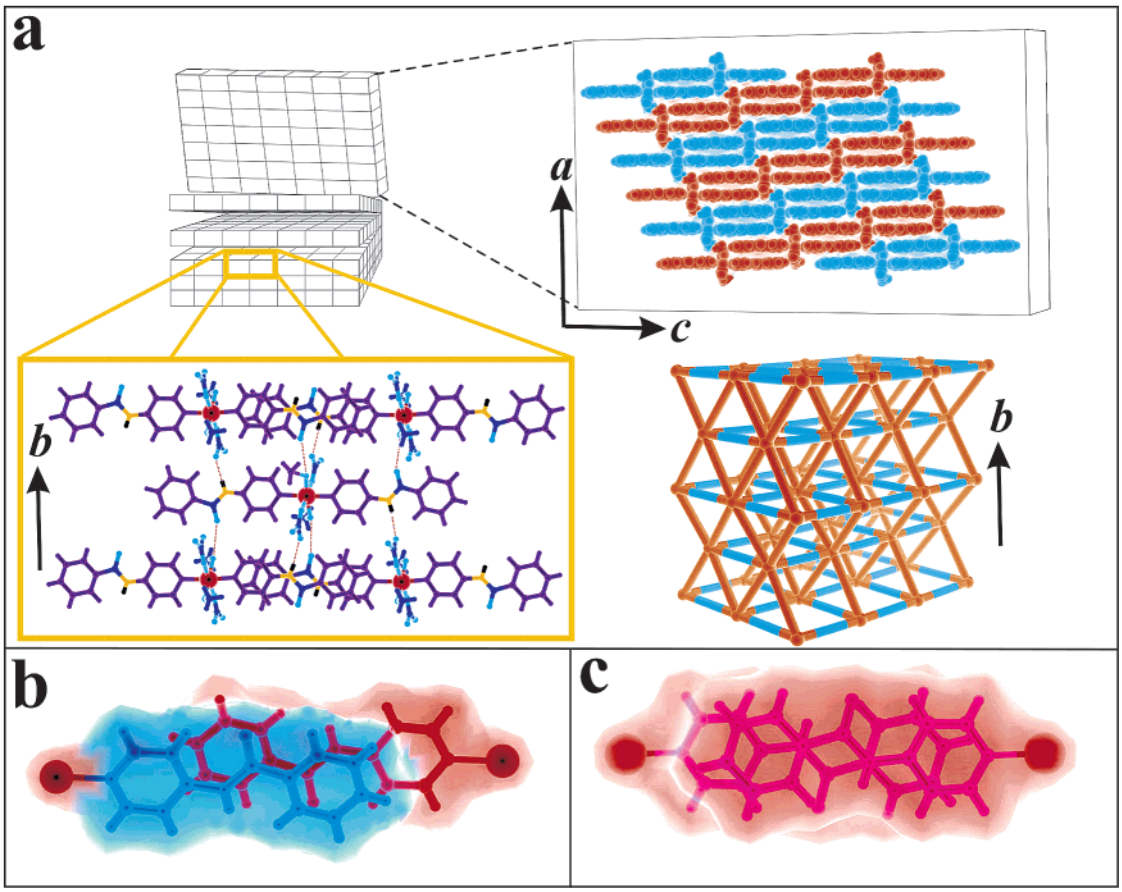

Figure 14. $M(NPBA)_2(NO_3)_2(MeOH)_2$, M = Co^{2+} (**7**), Ni^{2+} (**8**), and Zn^{2+} (**9**). (a) 2-D $\pi-\pi$ stacking networks with Type III and Type V $\pi-\pi$ stacking interactions propagate along the *ac* plane and interact via hydrogen bonding with other 2-D planes along *b*. Inset: Schematic structure of **7**−**9** (blue represents $\pi-\pi$ stacking networks and orange represents hydrogen bonding networks). (b) Type III $\pi-\pi$ stacking interactions (c) Type V $\pi-\pi$ stacking interactions.

atoms O(2)H of the coordinated methanol and the carbonyl groups C═O(1) of two adjacent units positioned opposite to one another and have average O−H···O contacts of 2.83 Å. The other intermolecular hydrogen bonds are between the amide groups N(2)H of the ligand and the noncoordinated oxygen atoms O(5) of the nitrate ions from another set of adjacent units, which are also opposite to one another, and have average N−H···O contacts of 3.04 Å. Both sets of interactions occur along *b* and propagate in two dimensions along the *bc* plane (Figure 14a and Table 2). The $\pi-\pi$ stacking networks of **7**−**9** comprise two types of $\pi-\pi$ interactions, Types III and V: the first consists of the stacking of adjacent benzamido groups and the second stacking between the entire structure of NPBA's of adjacent units with average contact distances of 3.43 and 3.59 Å, respectively, (Figure 14b,c and Table 3). The $\pi-\pi$ stacking system propagates along 2-D sheets that are parallel to the *ac* plane. Such 2-D sheets are one molecule thick and are linked by the hydrogen bonds that propagate along *b* generating an overall structure with a 3-D noncovalent network (Figure 14).

Octahedral *trans*-$Mn(NPBA)_2(NO_3)_2(H_2O)_2$ (**10**, Figure 15) exhibits a 3-D network also composed of hydrogen bonding and $\pi-\pi$ stacking interactions. Each unit interacts with 10 neighbors via 12 noncovalent interactions and forms the most complex 3-D network of the crystalline assemblies of NPBA, thus observed in the study. Intramolecular hydrogen bonds occur between the coordinated water O(2)H and the noncoordinating oxygen atoms O(5) of the nitrates with O−H···O contacts of 2.85 Å. There are three types of intermolecular hydrogen bonds.

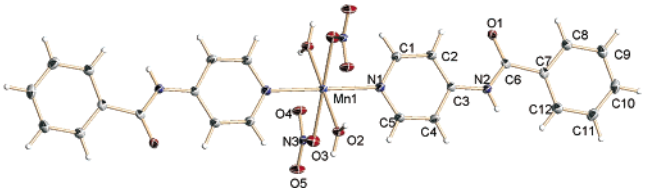

Figure 15. Structure of $Mn(NPBA)_2(NO_3)_2(H_2O)_2$, **10**.

One type consists of O−H···O contacts of 2.88 Å between the oxygen atoms O(2)H1 of the coordinated water and the noncoordinating oxygen atoms O(4) of the nitrates from two adjacent units along *a* (Figure 16d and Table 2). The two other types of intermolecular hydrogen bonds consist of O−H···O contacts of 2.73 Å between the oxygen atoms O(2)H2 of the coordinated water and the carbonyl groups C═O(1) and between the amide groups N(2)H and the noncoordinating oxygen atoms O(5) of the nitrates with N−H···O contacts of 3.01 Å, both of which occur with the next adjacent units along the *bc* plane (Figure 16c and Table 2). Complex **10** contains Type IV $\pi-\pi$ stacking interactions that arise from the stacking of phenyl and pyridyl moieties of adjacent units with average inter-ring contacts of 3.59 Å and propagate along the *ac* plane (Figure 16a,b and Table 3). The combination of the hydrogen bonding and $\pi-\pi$ stacking interactions in **10** generates a 3-D solid-state network composed of a 2-D $\pi-\pi$ stacking system overlapped with a 3-D hydrogen bonded network.

Ligand Geometry and Supramolecular Networks. NPBA has three planar regions, the pyridyl, the carboxamide, and the

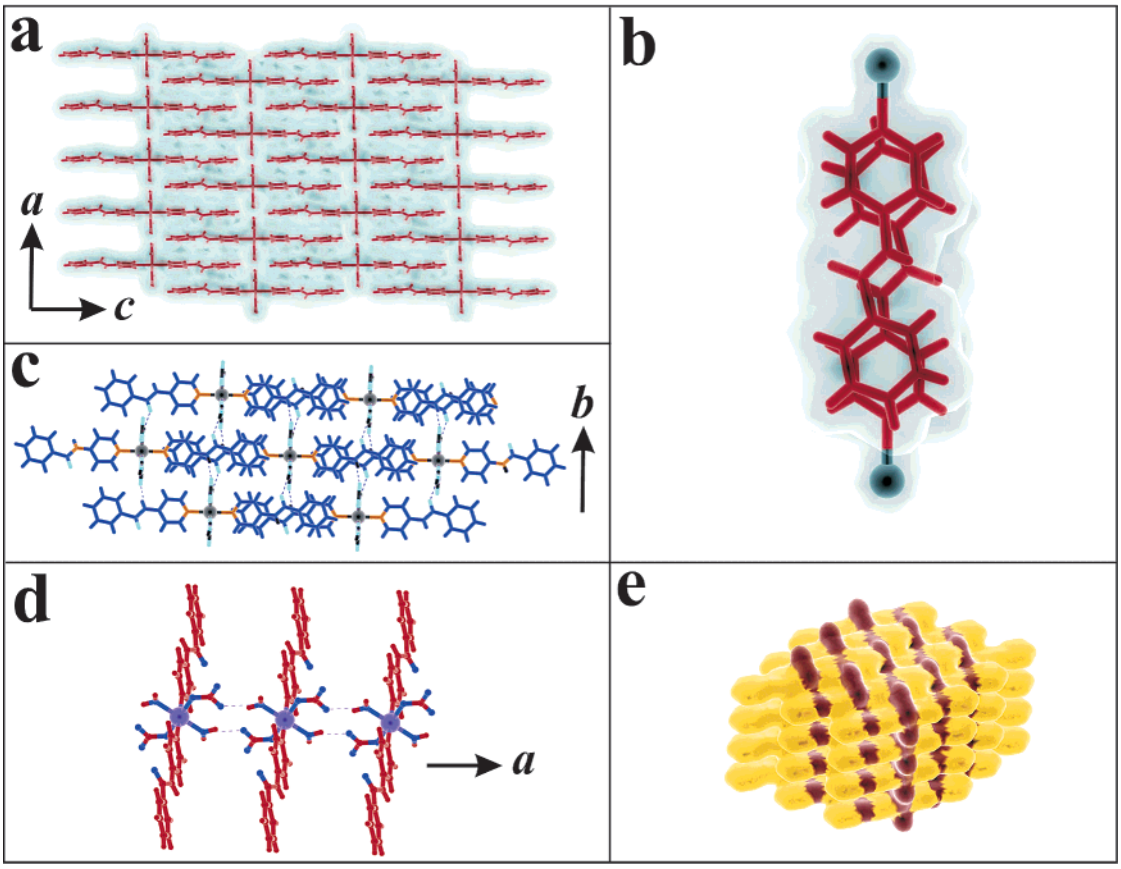

Figure 16. $Mn(NPBA)_2(NO_3)_2(H_2O)_2$, **10**. (a) 2-D $\pi-\pi$ stacking network comprised of (b) Type IV $\pi-\pi$ stacking interactions. (c) 2-D hydrogen bonding networks along the *bc* plane. (d) 1-D hydrogen bonding networks along *a*. (e) van der Waals surfaces of the 3-D noncovalent networks (red are hydrogen bonding networks and yellow are $\pi-\pi$ stacking networks).

phenyl group. Although conjugation through the whole ligand would make NPBA a rigid planar structure, the actual conformation deviates from the planarity due to network interactions. For example, the torsion angles Φ_1 and Φ_3 (Figure 1 and Table S2, Supporting Information) vary from $-34.3°$ to $+23.2°$, depending on the intermolecular contacts. These degrees of freedom in the ligand enable the formation of different directional noncovalent networks, since the flexibility adjusts to the local environment in order to promote the formation of the noncovalent networks.

Hydrogen-Bonding Networks. NPBA can serve as both a hydrogen bond donor and/or acceptor using the amide nitrogen atom and the carbonyl oxygen atom of the carboxamide group, respectively. However, in NPBA only the amide nitrogen atom serves as hydrogen bond donor and the pyridyl nitrogen, not the carbonyl group, is the hydrogen bond acceptor (Figure 2 and Table 2). In **2**−**4** and **6**, the amide nitrogen atoms are the only hydrogen bond donors and the acetates, nitrates, and the carbonyl groups of the ligand are the hydrogen bond acceptors. For example, in **2** the intermolecular hydrogen bond interactions are between the amide nitrogen and the oxygen atom of the nitrate anion (Figure 4 and Table 2). Similarly, in **3**, **4**, and **6** only intermolecular hydrogen bond interactions between the amide nitrogen and the oxygen of the anionic acetate ligands are observed (Figures 6, 8, and 12 and Table 2).

When solvent is present, the oxygen atom of the carboxamide group is involved in hydrogen bonding interactions with either the amide-NH donor of the ligand or hydroxyl-OH group of the solvent molecules. This type of network occurs in **5** and **7**−**10**. For example, in **5**, the amide nitrogen and carbonyl oxygen of the carboxamide group hydrogen bond and resemble those observed in the β-sheets of protein structures (Figure 10 and Table 2). In **7**−**9**, the hydrogen bonding interactions occur between the amide-NH group and the oxygen atoms of the nitrates along with the interactions between the methanol and the oxygen of the carbonyl groups (Figure 14 and Table 2). The hydrogen bonding in **10** is very similar to that in **7**−**9**, except that the added hydrogen bonding ability of the coordinated water generates a 3-D hydrogen bonding network (Figure 16 and Table 2).

Overall, hydrogen bonding interactions between the NPBA-bound units determine the structural motifs as the number of hydrogen bonds is maximized. In most cases, the directional aspect of the hydrogen bonding motifs from the scaffolds direct the formation of the infinite networks through various directions in the crystal structure.

***π*−*π* Stacking Networks.** No $\pi-\pi$ stacking interactions are observed in **1**, even though potentially three planar groups, pyridyl, carboxamide, and phenyl, are present in the ligand. Nonetheless, when the ligand binds to metal ions with various geometries, several types of $\pi-\pi$ stacking interactions propagate in unique ways through the structure. In these interactions, not only the phenyl group but also the pyridyl and the carboxamide groups participate in the $\pi-\pi$ stacking networks. For example, in **7**−**9**, all the pyridyl−carboxamide−phenyl moieties are involved in the $\pi-\pi$ stacking interactions, Type V (Figure 14 and Table 3), wherein all planar groups are in coplanar conformation (i.e., $\Phi_{1,3} \sim 0$, Table S2). This type of $\pi-\pi$

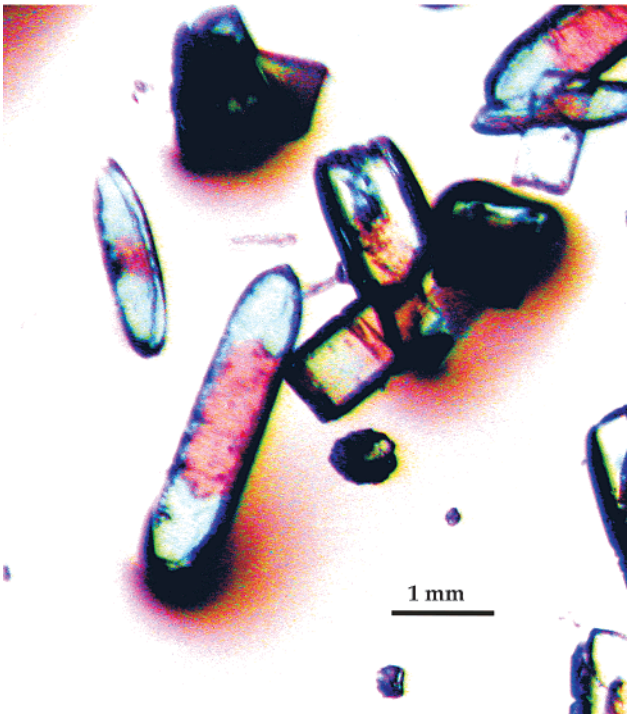

Figure 17. Optical microscopy image of two-component crystal composite **11** (red, Co-complex **7**; blue, Ni-complex **8**).

stacking interaction is the most extensive $\pi-\pi$ stacking possible in these systems. Another type of $\pi-\pi$ stacking interaction, Type IV, is observed between the pyridyl and phenyl groups and is present in **6** and **10** (Figures 12 and 16, respectively, and Table 3). This type of $\pi-\pi$ stacking interaction is similar to Type V, except that the ligands are to some extent displaced from each other and the stacking interaction is limited only within the pyridyl and phenyl groups. The third type of $\pi-\pi$ stacking interaction, Type III, is observed between the carboxamide-phenyl and phenyl-carboxamide groups in **5** (Figure 10) and **7**−**9** (Figure 14 and Table 3). The extent of the stacking interaction in Type III is much smaller than that in Type V, since only half of the ligand is involved in the stacking interaction. The forth type of $\pi-\pi$ stacking interaction, Type II, consists of the stacking of only the pyridyl groups. This type of $\pi-\pi$ stacking was observed in **3** and **4** (Figures 6 and 8, respectively, and Table 3). The fifth type of $\pi-\pi$ stacking interaction, Type I, is the weakest $\pi-\pi$ interactions and consists of the stacking of the amide-pyridyl moieties with the pyridyl groups of the ligand and is observed in **2** (Figure 4 and Table 3). In all cases, except **2**, $\pi-\pi$ stacking interactions occur when the ligands are in antiparallel orientations with one another. In **2**, the $\pi-\pi$ stacking interactions occur when the ligands are parallel.

The $\pi-\pi$ stacking interactions generated from the scaffolds derived from NPBA have large variations in terms of the extent and magnitude of their interactions. Thus, the $\pi-\pi$ stacking motifs, due to the diversity of their interactions, can be opportunistic noncovalent motifs that nevertheless can direct the formation of different kinds of noncovalent network motifs. Their importance is underlined by the fact that in **2**−**10**, $\pi-\pi$ stacking interactions established infinite networks throughout the structures.

Hydrogen Bonding Directed Topotaxy in 11 and 12. The fact that **7**−**9** are isomorphous prompted the study of their ability

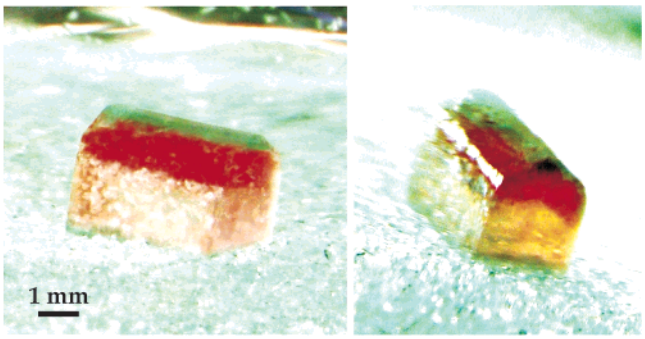

Figure 18. Optical microscope image of the three-component crystal composite **12**.

Scheme 2. Crystal Growth Along the Direction of the Hydrogen Bonding Networks in **7**−**9**

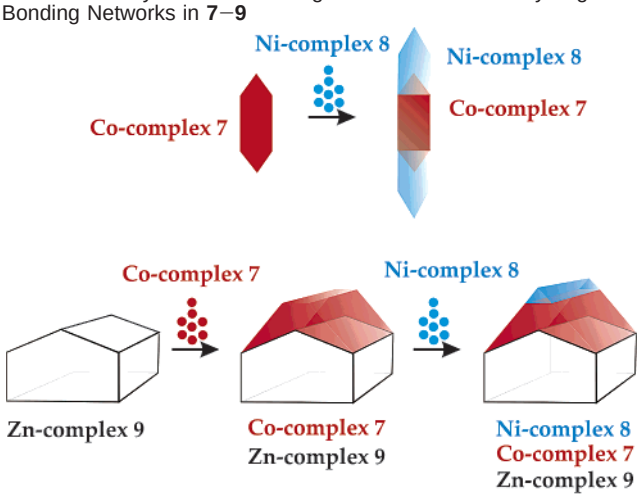

to grow one crystalline material on another. When single crystals of **7**, **8**, or **9** are used as seed crystals in toluene:methanol solutions of different isostructural members of their family, the seed crystals nucleate growth of a different material on the surfaces that coincide with *b*. For example, when single crystals of $Co(NPBA)_2(NO_3)_2(MeOH)_2$ (**7**) are placed in a 1.5 mM toluene:methanol solution of $Ni(NPBA)_2(NO_3)_2(MeOH)_2$ (**8**) followed by vapor diffusion of diethyl ether, the results are single crystals where **8** is grown along *b* in **7** (Figure 17), as illustrated in Scheme 2. Assignment of the crystallographic directions was based on the X-ray diffraction data from one of the single-crystal composites, which produced structure **11** (Table 1). Particularly interesting is that the growth predominantly takes place along *b* in **7**, which are the lattice planes that project an array of hydrogen-bonding elements in the assembly (Figure 14). Thus, the 2-D growth observed in **11** is a result of the perfect lattice match, as well as the strength and abundance of the hydrogen-bonding interactions along *b* in **7**−**9**.

In a similar way, we prepared a triple component crystal where **7**, **8**, and **9** formed a single crystal. Using the same method described above, subsequent crystallization of $Co(NPBA)_2(NO_3)_2(MeOH)_2$ (**7**) and $Ni(NPBA)_2(NO_3)_2(MeOH)_2$ (**8**) on single crystals of $Zn(NPBA)_2(NO_3)_2(MeOH)_2$ (**9**) resulted in the formation of a triple component crystal **12** (Figure 18). As in **11**, the single-directional topotaxial growth in **12** suggests that the growth propagates preferentially along *b*.

The molecular control of the nucleation of molecules on substrates is a rapidly growing area of research because it can play an important role in the formation of advanced crystalline

Scheme 3. Graphic Representation of the Formation of Crystalline Solid Solutions **13**−**16**

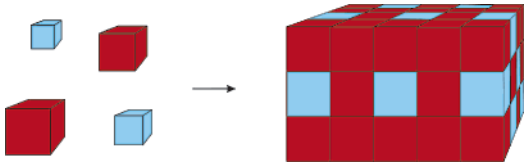

films for liquid crystal switches and displays, electroluminescent displays, and second-harmonic generation,[62] as well as for materials that can promote the nucleation of single crystals of selected polymorphs of pharmaceuticals, a concept recently demonstrated by Ward and co-workers.[63] Currently, some of the approaches that are being used to control the nucleation and growth of crystals are the design of growth interfaces such as polymers,[64] Langmuir monolayers,[65] organic salt crystals,[66] graphite,[67] organic single crystals,[68] and surfaces of metastable crystal phases.[69] At present, one of the most promising of these approaches is the epitaxial growth of molecules on crystal surfaces, since in this case epitaxy is governed by factors which can be known with atomic resolution such as topological structure, lattice parameters of ledge nucleation sites, symmetry constrains, the substrate crystal planes, and molecular composition of the aggregates.[70,71] Hydrogen bonding directed epitaxial growth of single crystals on crystal surfaces has been reported in the literature.[48,72] Crystals **11** and **12** represent new examples where the direction of topotaxy is directed by hydrogen bonding networks.

Solid Solutions of 7−**9.** The isomorphous nature of **7**−**9** also prompted the exploration of their ability to form solid solutions of **7**−**9**; this concept is illustrated in Scheme 3. Similar procedures have been applied in the past for the formation of solid solutions with mixed metals.[48] Solid solutions with varying metal compositions of Co(II), Ni(II), and Zn(II), i.e., **13** (Co:Ni, 75:25), **14** (Co:Ni, 50:50), **15** (Co:Ni, 25:75), and **16** (Ni:Zn, 50:50), were made. Analysis of these crystals via X-ray powder diffraction, magnetic susceptibilities, and elemental analysis revealed that these solid solutions are isomorphous and may be useful for the fine-tuning of the properties of crystals, for example, to control the conductivity, index of refraction, and color of materials with high precision.

Magnetic Properties of 4, 5, 7, 8, 10, and Solid Solutions 13−**16.** The magnetic susceptibility, χ, of **4**, **5**, **7**, **8**, **10**, and **13**−**16** was measured between temperatures of 2 and 300 K using a SQUID magnetometer, and plotted as $\mu_{eff}(T) = [(8\chi T)^{1/2}]$ (Figures 19 and 20). For the 1-D Cu(NPBA)$_2$(OAc)$_2$ (**4**), the

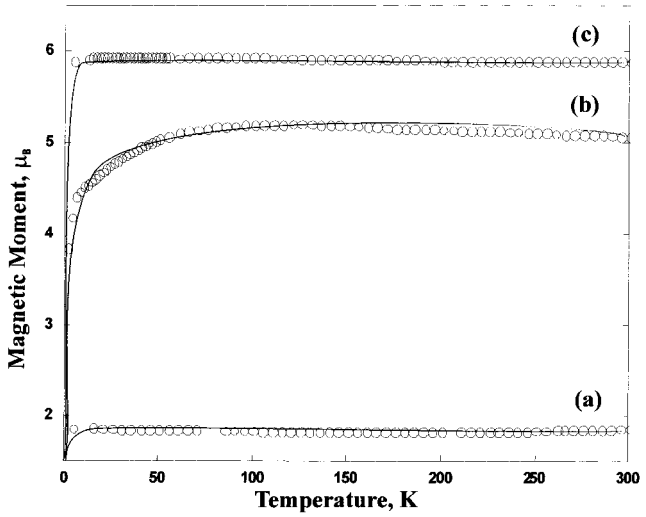

Figure 19. Temperature dependence of the effective magnetic moment for (a) Cu-complex **4**, (b) Co-complex **5**, and (c) Mn-complex **10**. Note that the solid lines are fits discussed in the text.

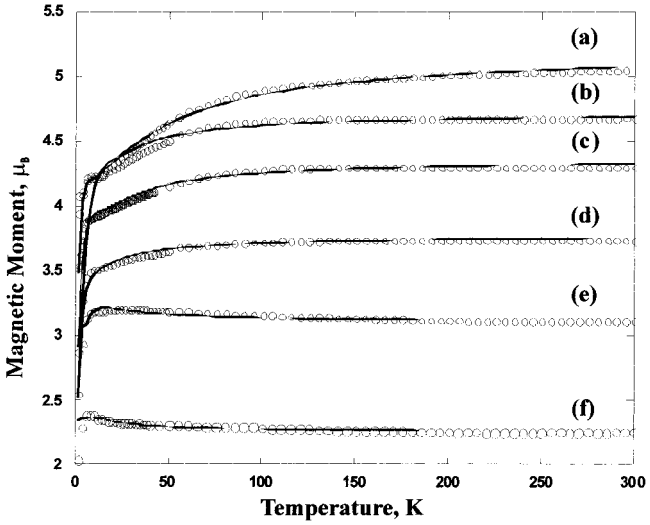

Figure 20. Temperature dependence of the effective magnetic moment for (a) Co-complex **7**, solid solutions (b) **13**, (c) **14**, and (d) **15**, (e) Ni-complex **8**, and solid solution (f) **16**.

300 K μ_{eff} is 1.86 μ_B, consistent with it having a g value of 2.15. The temperature-dependent magnetic properties follow simple Curie−Weiss behavior, $\chi \propto (T - \theta)^{-1}$, with $\theta = -0.2$, and again $g = 2.15$, indicating no interactions between the Cu(II) metal centers. For the 2-D Co(NPBA)$_2$(OAc)$_2$(H$_2$O)$_2$ (**5**), its room temperature magnetic moment of μ_{eff} is 5.06 μ_B, and exceeds the expected spin-only values of 3.87 μ_B. The high-temperature deviation is attributed to the Lande g-values deviating from the typical value of 2 due to the spin−orbit coupling, while the deviation at low temperature is attributed to zero-field splitting (D) of the metal ions. The $\chi(T)$ was fit to expressions that account for D for Co(II), eq 1 for the $S = {}^3/_2$ Co(II),[73] where N is Avogadro's number, and θ accounts for weak interactions between Co(II) sites. Thus, Co(NPBA)$_2$(OAc)$_2$(H$_2$O)$_2$ (**5**) can be modeled to eq 1 with $g = 3.30$, $D = 10$ cm^{-1} (14.4 K), and $\theta = -2$ K. The small θ value is consistent with weak antiferromagnetic nearest neighbor spin coupling.

(62) For a review see: Marks, T. J.; Ratner, M. A. *Angew. Chem., Int. Ed. Engl.* **1995**, *34*, 155.
(63) Mitchell, C. A.; Yu, L.; Ward, M. D. *J. Am. Chem. Soc.* **2001**, *123*, 10830.
(64) Damman, P.; Dosière, M.; Smith, P.; Wittmann, J. C. *J. Am. Chem. Soc.* **1993**, *117*, 1117.
(65) Frostman, L. M.; Ward, M. D. *Langmuir* **1997**, *13*, 330.
(66) DaCosta, V.; Le Moigne, J.; Oswald, L.; Pham, T. A.; Thierry, A. *Macromolecules* **1998**, *31*, 1635.
(67) Last, J. A.; Hillier, A. C.; Hooks, D. E.; Maxson, J. B.; Ward, M. D. *Chem. Mater.* **1998**, *10*, 422.
(68) Carter, P. W.; Ward, M. D. *J. Am. Chem. Soc.* **1993**, *115*, 11521.
(69) Rodríguez-Hornedo, N.; Lechuga-Ballesteros, D.; Wu, H.-J. *Int. J. Pharm.* **1992**, *85*, 149.
(70) For a review see: Ward, M. D. *Chem. Rev.* **2001**, *101*, 1697.
(71) Hooks, D. E.; Fritz, T.; Ward, M. D. *Adv. Mater.* **2001**, *13*, 227.
(72) E.g.: (a) Carter, P. W.; Ward, M. D. *J. Am. Chem. Soc.* **1994**, *116*, 769. (b) Krober, J.; Codjovi, E.; Kahn, O.; Groliere, O.; Jay, C. J. *Am. Chem. Soc.* **1993**, *115*, 9810. (c) Ohkoshi, S.; Iyoda, T.; Fujishima, A.; Hashimoto, K.; *Phys. Rev.* **1997**, *56*, 11642. (d) Ohkoshi, S.; Fujishima, A.; Hashimoto, K. *J. Am. Chem. Soc.* **1998**, *120*, 5349. (e) Mizuno, M.; Ohkoshi, S.; Hashimoto, K. *Adv. Mater.* **2000**, *12*, 1955.
(73) O'Connor, C. J. *Prog. Inorg. Chem.* **1982**, *29*, 1205.

$$\chi_{Co} = \frac{N\mu_B{}^2 g_{Co}{}^2}{3k_B(T-\theta)} \frac{1+9e^{-2D_{Co}/k_BT}}{4(1+e^{-2D_{Co}/k_BT})} + \frac{2N\mu_B{}^2 g_{Co}{}^2}{3k_B(T-\theta)} \frac{4+\frac{3k_BT}{D_{Co}}(1-e^{-2D_{Co}/k_BT})}{4(1+e^{-2D_{Co}/k_BT})} \quad (1)$$

In the 3-D $Co(NPBA)_2(NO_3)_2(MeOH)_2$ (**7**), with a similar $\mu_{eff} = 5.08\ \mu_B$, the temperature-dependent magnetic behavior can be modeled with eq 1 as well but with values of $g = 3.30$, $D = 30\ cm^{-1}$ (43 K), and $\theta = -6$ K, indicating similar antiferromagnetic interactions to those present in $Co(NPBA)_2(OAc)_2(H_2O)_2$ (**5**), but with slight variances at lower temperatures due to a greater *D*. A similar behavior is observed for the isostructural $Ni(NPBA)_2(NO_3)_2(MeOH)_2$ (**8**), which has a 300 K $\mu_{eff} = 3.12\ \mu_B$ and is best modeled with eq 2 for the $S = 1$ Ni(II) center with $g = 2.20$, $D = 18\ cm^{-1}$ (26 K), and $\theta = 2$ K. For Co-complex **7** and Ni-complex **8**, the small θ values are consistent with a weak antiferromagnetic and ferromagnetic, respectively, nearest neighbor spin coupling. The manganese containing 3-D **10,** which has a 300 K $\mu_{eff} = 5.88\ \mu_B$, follows simple Curie−Weiss behavior with $\theta = -0.1$ K, and exhibits a *g* value of 1.99. In this case, despite the extensive intermolecular interactions present in **10**, the magnetic properties appear to be more dependent on metal−metal distances than the number of interactions between the metal complexes.

$$\chi_{Ni} = \frac{N\mu_B{}^2 g_{Ni}{}^2}{3k_B(T-\theta)} \frac{2e^{-D_{Ni}/k_BT}}{1+2e^{-D_{Ni}/k_BT}} + \frac{2N\mu_B{}^2 g_{Ni}{}^2}{3k_B(T-\theta)} \frac{\frac{2k_BT}{D_{Ni}}(1-e^{-D_{Ni}/k_BT})}{1+2e^{-D_{Ni}/k_BT}} \quad (2)$$

Solid solutions **13**−**15** with a $[Co_yNi_{1-y}(NPBA)_2(NO_3)_2(MeOH)_2]$ composition exhibit magnetic properties in relation of the proportion of their metal content, with little perturbation of the interactions between metal centers. The magnetic properties of these materials can be best fit with a linear combination of eq 1 and 2, i.e., eq 3, where *y* is the fraction of Co(II) ions in the sample (Figure 20).

$$\chi_{total} = (y)\chi_{Co} + (1-y)\chi_{Ni} \quad (3)$$

The Co:Ni samples with 3:1, 1:1, and 1:3 ratios could be modeled with $g_{Co} = 3.35 \pm 0.05$, $g_{Ni} = 2.20$, $D_{Co} = 20 \pm 5\ cm^{-1}$, and $D_{Ni} = 8 \pm 2\ cm^{-1}$. The same θ value of -2 K was used in eq 1 and 2, thus becoming an average value of Ni−Ni, Ni−Co, and Co−Co interactions in the solids, which again shows weak magnetic coupling between metal centers within the structure. Likewise, solid solution **16** that contains the Ni-complex **8** and Zn-complex **9** at a 1:1 ratio can also be modeled to exactly one-half of eq 2, with $g_{Ni} = 2.20$, $D_{Ni} = 14\ cm^{-1}$ (26 K), and $\theta = 2$ K, as $S = 0$ Zn(II) does not contribute to the magnetic behavior. There is little difference in the overall magnetic behavior of the Ni:Zn mixture compared to the pure Ni(II) complex **8**; however, only slight changes in the *D*-value are observed which may be attributed to slight orientation effects within the crystal lattice.

Conclusion

Herein we reported a set of new structural scaffolds based on metal complexes of *N*-(4-pyridyl)benzamide that generate crystalline solids with 1-, 2, and 3-D networks of hydrogen bonding and $\pi-\pi$ stacking interactions. The dimensionality of the noncovalent networks in structures **2**−**10** is determined by the directional noncovalent motifs of the units. 1-D networks of hydrogen bonding and $\pi-\pi$ stacking interactions were observed in Ag-complex **2**, Zn-complex **3**, and Cu-complex **4**. Co-complex **5** comprised a pair of 1-D networks of hydrogen bonding and $\pi-\pi$ stacking interactions that run perpendicular to one another and form 2-D noncovalent networks. In the Zn-complex **6**, although it also comprises two 1-D networks of hydrogen bonding and $\pi-\pi$ stacking interactions that run perpendicular to one another, the overall structure exhibits a 3-D noncovalent network system as the individual networks interact with one another in a zigzag fashion along the third dimension of space. Co-complex **7**, Ni-complex **8**, and Zn-complexe **9** are isostructural and generate 3-D noncovalent network structures. They comprise a 2-D $\pi-\pi$ stacking system that forms sheets with arrays of hydrogen bonding groups oriented orthogonally and which ultimately join the sheets together to form a 3-D solid network. Due to their isomorphous nature, topotaxial growth of single crystals of any member (**7**−**9**) enables the growth of mixed single crystals, **11** and **12**, as well solid solutions **13**−**16**. Mn-complex **10** exhibits a 3-D noncovalent network composed of 3-D hydrogen bonding systems that overlaps with a 2-D $\pi-\pi$ stacking system in a very similar way as **7**−**9**. The temperature-dependent magnetic moment measurements of paramagnetic assemblies **4**, **5**, **7**, **8**, and **10** and the solid solutions **13**−**16** were obtained between 2 and 300 K. They indicated that minor interactions are observed for the assemblies that exhibit higher dimensional networks of noncovalent interactions, namely **5**, **7**, **8**, and **13**−**16**.

Acknowledgment. We thank Dr. Lesley Sieburth for her assistance with the photographic work of the crystal composites. Financial support by the National Institute of Health (Grant No. 5R01GM57052), the National Science Foundation (Grant Nos. CHE-9818472 and CHE-9320478), the U.S. Department of Energy (Grant No. DE FG 03-93ER45504), and the NIH Research Supplement for Dr. Juan C. Noveron are gratefully acknowledged. Dedicated to the memory of Professor Donald J. Cram for his pioneering contributions in supramolecular chemistry.

Supporting Information Available: Tables of bond lengths (Å) and angles (deg) around the metal ions and conformation angles Φ_1, Φ_2, and Φ_3 of NPBA (PDF) and additional crystallographic data for **1**−**11** (CIF). This material is available free of charge via the Internet at http://pubs.acs.org.

JA0200241